RSC Advances




ROYAL SOCIETY OF CHEMISTRY

www.rsc.org/advances

## Table of contents entry

The $Fe_3O_4$/N-GAs directly derived from Fc-F/GO supramolecular hydrogels act as multifunctional reagents, including Fe/N sources and the dispersant of GO.

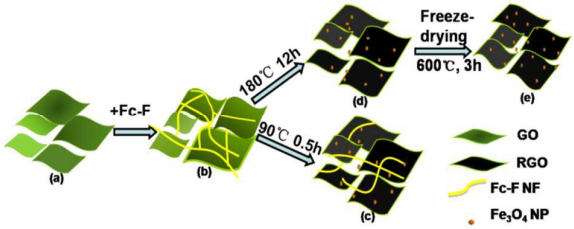

RSC Advances

PAPER

# From supramolecular hydrogels to functional aerogels: a facile strategy to fabricate $Fe_3O_4$/N-doped graphene composites

Received 00th January 20xx,
Accepted 00th January 20xx

DOI: 10.1039/x0xx00000x

www.rsc.org/

Ting He,[a] Zhengyuan Li,[a] Zhifang Sun,[a] Shuzhen Chen,[a] Rujuan Shen,[b] Lunzhao Yi,[c] Liu Deng,*[,a] Minghui Yang,[a] Hongtao Liu[a] and Yi Zhang*[,a]

This manuscript introduces a simple method to fabricate hybrid aerogels with $Fe_3O_4$ nanocrystals/nitrogen-doped graphene ($Fe_3O_4$/N-GAs) through one-shot self-mineralization of ferrocenoyl phenylalanine/graphene oxide (Fc-F/GO) supramolecular hydrogels. We found that GO could trigger a sol-gel transition of Fc-F gelators below the critical gelation concentration and the electron microscopic results revealed that the self-assembled Fc-F fibrils tightly bound onto graphene sheets. Upon the hydrothermal reaction, Fc moieties in these fibrils could be locally oxidized to $Fe_3O_4$ nanocrystals by GO, retaining on the top of reduced GO (RGO) sheets and therefore inhibiting the self-aggregation of graphene nanosheets. After drying, the remains of supramolecular hybrid hydrogels presented as the three-dimensional (3D) framework of ultra-thin graphene sheets on which $Fe_3O_4$ nanoparticles (NPs) uniformly immobilized as single crystals. Since the new born $Fe_3O_4$ nanocrystals closely anchored on the graphene sheets, the as-prepared $Fe_3O_4$/N-GAs complex shows excellent electrocatalytic activity to the oxygen reduction reaction (ORR, comparing to the commercial Pt/C). Notably, the Fc-F/GO supramolecular hydrogels act as multifunctional reagents, such as the capping agent for preventing graphene nanosheets from stacking and the Fe and N sources for $Fe_3O_4$/N-GAs. We expect that this intriguing strategy can provide a useful archetypical example in designing nonprecious metal oxides/carbon hybrid materials to serve as substitutes for noble metal catalysts.

## Introduction

The development of high efficient ORR catalysts has been widely considered as a key issue in energy conversion technologies.[1-6] Traditional ORR electrocatalysts usually contain precious metals like platinum, gold, palladium, etc. However, the prohibitive cost and scarce supply of these precious metal catalysts limit their large-scale application.[7-10] Therefore, alternative ORR catalysts with high catalytic activity but low cost are highly desired. The heteroatom-doped carbon materials have been regarded as the promising type of ORR catalysts. Among them, the N-doped graphene materials have been considered as the hottest topic for investigating heteroatom-doped carbon materials as ORR catalysts.[11-15] Comparing to the porous N-graphene materials which is constructed by randomly stacked N-graphene sheets, the N-GAs possess much higher electronic conductivity as a result of the continuous graphene sheets in the 3D networks, facilitating much faster charge transport across graphene sheet junctions.[16-18]

From another point of view, non-precious metals, metal oxides, metal chalcogenides and metal-$N_4$ structured macrocyclic compounds have also been applied to improve ORR catalytic activity.[19-24] The transition metal oxides, such as $Fe_2O_3$, $Fe_3O_4$ and $Co_3O_4$ have been convinced as important categories.[25-29] It is a pity that these metal oxides frequently suffer from dissolution, sintering and agglomeration, which would induce the catalyst degradation. Besides, the insulating property of the metal oxide further limits electrochemical reaction kinetics. Hence, various strategies have been developed to improve their structural integrity and electronic conductivity. Dai's group reported that $Co_3O_4$/graphene hybrids can be prepared through a general two-step method. In the first step, $Co_3O_4$ NPs were grown on GO sheets in the presence of $NH_4OH$. Subsequent hydrothermal reaction induced the crystallization of $Co_3O_4$ and reduction of GO to graphene.[28] The ZnO-coated 3D graphene aerogel templates

[a] College of Chemistry and Chemical Engineering, Central South University, Changsha 410083, China.
E-mail: yzhangcsu@csu.edu.cn (Yi Zhang), dengliu@csu.edu.cn (Liu Deng)
[b] State Key Laboratory of Power Metallurgy, Central South University, Changsha 410083, China.
[c] Yunnan Food Safety Research Institute，Kunming University of Science and Technology Kunming, 650500 (China)

Electronic Supplementary Information (ESI) available: additional electron microscopy images, CV curves and so on. See DOI: 10.1039/x0xx00000x

have been also proposed to prepare $Fe_3O_4$ NPs/graphene aerogels via a precipitation reaction in which $Fe_3O_4$ NPs replaced ZnO NPs.[18] However, despite these efforts, most of metal oxides/graphene nanocomposites exhibit lower activity and poorer conductivity than Pt-based materials.

The combination of transition metal oxides and N-GAs has been demonstrated to be a prospective approach. Such hybrid systems permit the use of advanced properties of both materials, such as high activity of transition metal oxides, rich porosity, 3D conductive networks and excellent mechanical properties of porous graphene films. Recently, a number of smart protocols have been successfully utilized to prepare $Fe_3O_4$/N-GAs with perfectly chemical performances. Müllen's group have described the assembly of $Fe_3O_4$ NPs in 3D N-GAs via hydrothermally treating the mixture of iron acetate, polypyrrole and GO solution at 180 °C, and then the hybrid system was dehydrated via a freeze-drying process and heated at 600 °C for $Fe_3O_4$ NPs crystallization.[26] The polypyrrole was introduced as a capping agent for both doping N and preventing graphene nanosheets from stacking.[30] This work demonstrates that N-GA is indeed a promising scaffold to improve the catalytic activity and durability of metal oxide NPs. So far, the traditional synthetic strategies for the metal oxides/N-doped carbon materials are generally involving two different ingredients to provide the metal oxides and N sources separately, resulting poor physical contact between the two active substances.[16, 31-33] In contrast, an *in situ* fabricating method of metal oxides/N-doped carbon nanomaterials derived from one precursor is highly desired to reduce the space barrier of electron transport.

This paper introduces a convenient fabricating route for preparing $Fe_3O_4$/N-doped graphene aerogels directly from supramolecular hybrid hydrogels. The as-prepared $Fe_3O_4$ NPs/N-GAs exhibit remarkable catalytic activity toward ORR. As far as we know, there is no report regarding supramolecular hydrogelators for the controllable self-assembly of metal oxide NPs and the doping N on graphene sheets. A single hydrogelator, Fc-F serves as a multifunctional reagent, not only for the Fe and N sources of both $Fe_3O_4$ NPs and N-doping graphenes, but also the dispersing agent for preventing graphene nanosheets from stacking. Therefore, the synergistic effect can be optimized by the close location of *in situ* formed N-graphenes and $Fe_3O_4$ NPs catalytic sites.[34-38] More significantly, the locally formation of metal oxides/N-GAs derived from supramolecular hydrogels offers a new route to produce the morphology-controlled inorganic NPs in hybrid graphene nanomaterials.

## Results and discussion

### Synthesis and Characterization of Supramolecular Hydrogels

In this paper, we chose a hydrogelator (Fc-F) to implement our proposal, since ferrocene and phenlyalanine could be able to act as Fe and N precursors, respectively.[39-42] The procedure for preparing the hybrid aerogel is briefly illustrated in Fig. 1.

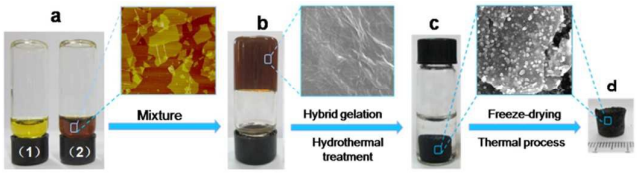


**Fig. 1** The fabrication process for the $Fe_3O_4$/N-GAs and corresponding electron microscopic images. (a) 2 mg $mL^{-1}$ Fc-F solution (1) and 1 mg $mL^{-1}$ GO solution (2); (b) Fc-F/GO hybrid hydrogels containing 2 mg $mL^{-1}$ Fc-F and 1 mg $mL^{-1}$ GO; (c) the Fc-F/GO hybrid hydrogels after hydrothermal treatment (180 °C, 12 h); (d) hybrid graphene aerogels after thermal process (600 °C, 3 h).

Initially, Fc-F/GO hydrogels were obtained by mixing the Fc-F with GO aqueous suspension (2 mg $mL^{-1}$ Fc-F and 1 mg $mL^{-1}$ GO, Fig. 1a-1b). After hydrothermal assembly, the supramolecular hybrid hydrogels were subjected to freeze-drying and further thermal treatment to fabricate the hybrid aerogels (Fig. 1c-1d). The structures and morphologies of hybrid Fc-F/GO hydrogels were investigated via the scanning electron microscopy (SEM), transmission electron microscopy (TEM) and atomic force microscopy (AFM). Fig. 2a-2b and Fig. S1 present the microscopic images of Fc-F spheres (2 mg $mL^{-1}$), GO sheets (1 mg $mL^{-1}$) and pure Fc-F hydrogels, respectively. Fc-F spheres can aggregate into Fc-F fibrils after the addition of GO. As shown in Fig. 3a-3b, the diameter of these Fc-F fibrils in the hybrid system is around 50-100 nm, while the length of these fibrils reaches 1 mm (or longer). Apparently, the Fc-F fibrils and GO nanosheets interlaced with each other in the hybrid hydrogel system. On the one hand, the required concentration of Fc-F applied in forming Fc-F/GO hybrid hydrogels can be significantly lower than the critical gelation concentration with respect to pure Fc-F hydrogels (3.0 mg $mL^{-1}$), indicating that GO serves as a positive co-gelator besides a solid matrix. On the other hand, the mixture containing enough GO but much

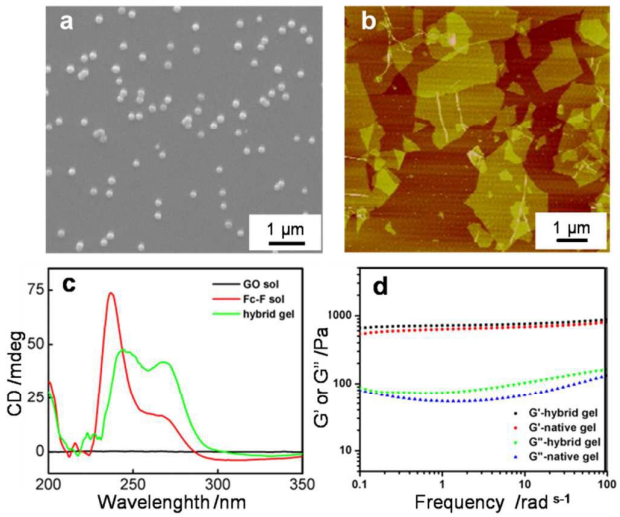


**Fig. 2** The SEM image of 2 mg $mL^{-1}$ Fc-F (a) and AFM image of 1 mg $mL^{-1}$ GO (b); (c) CD spectra of GO solution, Fc-F solution and hybrid hydrogels contained 2 mg $mL^{-1}$ Fc-F, respectively; (d) Dynamic frequency sweep of hybrid hydrogels and Fc-F native hydrogels.

less Fc-F (less than 2.0 mg $mL^{-1}$) cannot form stable hybrid hydrogels, so the Fc-F plays a critical role in facilitating the formation of the mixed hydrogels. Circular dichrosim (CD) spectrum was also used to characterize the conformational information of Fc-F/GO hybrid hydrogels.[43, 44] As shown in Fig. 2c, the hybrid Fc-F/GO hydrogels obviously inherited the chirality derived from Fc-F hydrogels.[39-42, 45] It is notable that for the hybrid hydrogels, the intensity of the first peak (around 240 nm) decreased while the second peak (around 270 nm) increased comparing with that for the pure Fc-F sol, implying the helix conformation of Fc-F fibrils. Additionally, we explored the viscoelastic properties of the hybrid hydrogels and native hydrogels ($C_{Fc\text{-}F}$ = 5 mg $mL^{-1}$) by measuring the storage modulus G' and the loss modulus G". As displayed in Fig. 2d, it can be seen that the viscoelastic properties of the two hydrogels are quite similar and the G' is about six times higher than G", indicating middle-strength hydrogels.[42]

**Fabrication and Characterization of $Fe_3O_4$/N-GAs**

After being hydrothermally incubated at 90 °C for 30 minutes, the color of Fc-F/GO hydrogels changed from brown to black, suggesting the reduction reaction of GO to graphene. On the basis of previous reports, GO exhibits strong oxidative ability to Fe(Ⅱ), so the Fc moiety in Fc-F fibrils could be oxidized to $Fe_3O_4$ NPs.[46, 47] Moreover, Fc-F fibrils could also act as a dispersant to prevent stacking of the graphene in the hydrothermal reduction process by weakening the bonding interaction between graphene sheets. In this way, $Fe_3O_4$ NPs could nucleate and grow on the graphene surface with simultaneous reduction of GO. The growth of $Fe_3O_4$ nanocrystals on graphene sheets was confirmed by TEM images. It is notable that Fc-F fibrils disappear, while an interconnected graphene framework co-existing with the small mineralized NPs (with sizes of 10-20 nm) is observed, confirming the effective coupling between the NPs and the graphene sheets (Fig. 3c). However, this well-structured nanomaterials exhibit poor catalytic ability to ORR (results are not shown). Thus for purpose of enhancing the composites catalytic activity, a higher temperature incubation process (heated at 600 °C for 3 h under $N_2$ protection) was performed. Our experimental results confirmed that the high temperature incubation process had little influence on the morphology of dehydrated nanocomplexes.

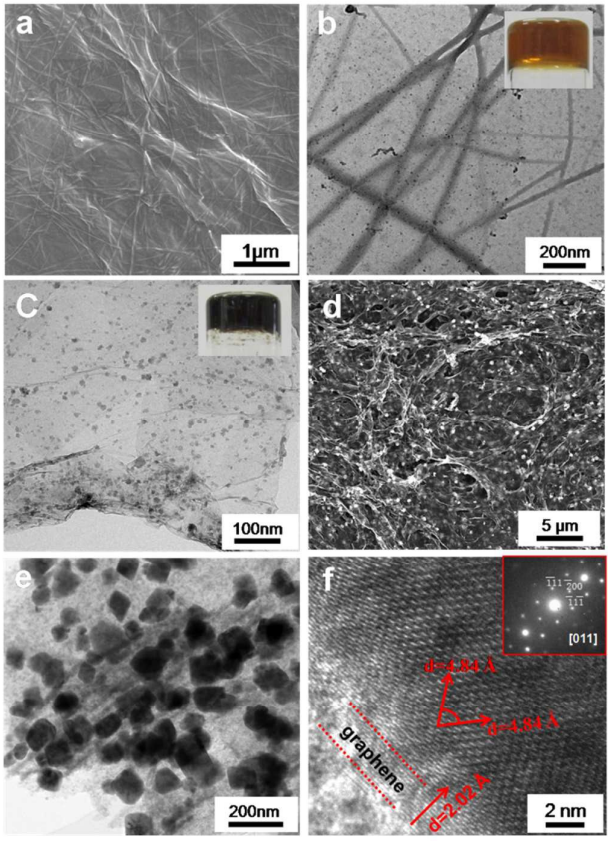


**Fig. 3** Morphologic images of Fc-F/GO hybrid hydrogels and $Fe_3O_4$/N-GAs. The SEM image (a) and TEM image (b) of Fc-F/GO hydrogels; TEM images of $Fe_3O_4$/N-GAs obtained by hydrothermal treatment at 90 °C for 30 minutes (c); The SEM image (d) and TEM image (e) of $Fe_3O_4$/N-GAs obtained by hydrothermal treatment at 180 °C for 12 h and annealed at 600 °C for 3 h under nitrogen protection; (f) The HRTEM image and (the inset) the SAED pattern of a $Fe_3O_4$ NP in GAs, recorded along the (011) direction.

To our knowledge, the optimized operation condition is to hydrothermally incubate the Fc-F/GO hydrogels at 180 °C for 12 h. Subsequent thermal treatment at 600 °C leads to the incorporation of N species into the graphene lattice. The final product is a black monolithic hybrid aerogel composed of N-doped graphene networks and $Fe_3O_4$ NPs, which has a low desity of 9.30 mg $cm^{-3}$ (Fig. 1d and Table S1). SEM images reveal that the obtained graphene sheets are thicker and more rigid (Fig. 3d and Fig. S2). The mineralized $Fe_3O_4$ NPs significantly grew up (with sizes of 50-100 nm) and uniformly dispersed on the graphene surfaces. Such kind of local engagement of metal oxide NPs within graphene skeletons reinforces the interfacial contact between NPs and graphene layers. Therefore, the self-agglomerations of both NPs and graphene sheets are inhibited, which promoting the electrochemical activity and stability of the composites.[48, 49] The TEM characterization further validates the uniform distribution of $Fe_3O_4$ NPs on the graphene (Fig. 3e). Interestingly, this method can uniquely yield $Fe_3O_4$ single crystals on the graphene surface. High-resolution TEM (HRTEM) reveals a typical $Fe_3O_4$ NP with a single-crystalline texture, which is entirely encapsulated by graphene sheets, belongs to a cubic system with lattice parameters of $a$=8.391Å (Fig. 3f). The lattice observation demonstrates that the two orientations (indexed to the $(\bar{1}1\bar{1})$ surface and the $(\bar{1}\bar{1}1)$ surface, respectively) with the same lattice spacing of 4.844 Å are rotated by 70.5° from one another. And the corresponding selected area electron diffraction (SAED) pattern recorded along (011) direction is shown in the inset (Fig. 3f).[50] Meanwhile, the typical hexagonal graphene construction with a lattice spacing of 2.02 Å (indexed to the (002) facet) is also observed.

Fig. 4a-f show the high-angle annular dark field scanning TEM (HAADF-STEM) image and HAADF-STEM/energy-dispersive X-ray spectroscopy (HAADF-STEM-EDS) maps of the

$Fe_3O_4$/N-GAs, respectively. It can be seen that the C and N elements are widely distributed all over the graphene surface, while the Fe and O elements are mainly located in the core of particles. Elemental distribution of a representative $Fe_3O_4$ NP was investigated by HAADF-STEM-EDS mapping, as shown in Fig. 5a-e. It is clear that Fe and O (light blue and dark blue) concentrate in the region where NPs are located, whereas C and N (red and green) spread everywhere. The $Fe_3O_4$/N-GAs nanocomposites were further analyzed by compositional linear scan with a higher spatial resolution across a single NP. Fig. 5f shows that C and N are evenly distributed across the whole surface, while Fe and O concenter on the core. Evidently, the N-doping sites and $Fe_3O_4$ are locally distributed on the graphene surface, which is crucial for the high catalytic performance towards ORR.[26]

X-ray powder diffraction (XRD) and X-ray photoelectron spectrum (or specta) (XPS) were also carried out to further identify the components of the oxidized products of supramolecular hydrogels. The XRD pattern confirms the existence of magnetic $Fe_3O_4$ NPs (JCPDS no. 65-3107) after thermal treatment at 600 °C (Fig. 6a). The diffraction peak at 20–30° with a *d-spacing* of 2.03 Å is assigned to the (002) surface of hexagonal graphene (2θ=26°), which is similar to the HRTEM result of $Fe_3O_4$/N-GAs ($d_{002}$=2.02 Å, Fig. 3f).[51] These results agree well with previous reports that Fc moiety can be stoichiometrically oxidized to $Fe_3O_4$ by GO.[46, 47] Meanwhile, XPS exhibits clear Fe 2p signals corresponding to the binding energy of Fe $2p_{1/2}$ and Fe $2p_{3/2}$ for $Fe_3O_4$ at 725 and 711 eV, respectively (Fig. S3 and Fig. 4g). This is consistent with the XRD results, further confirming that $Fe_3O_4$ NPs have been

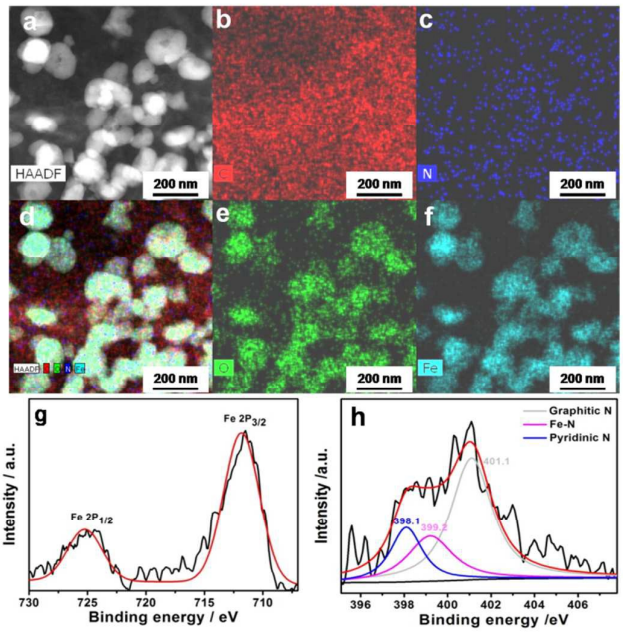


**Fig. 4** (a-f) The HAADF-STEM image, HAADF-STEM-EDS maps and (g) the XRD pattern of $Fe_3O_4$/N-GAs; XPS analysis of $Fe_3O_4$/N-GAs: (g) Fe 2p; (h) N 1s.

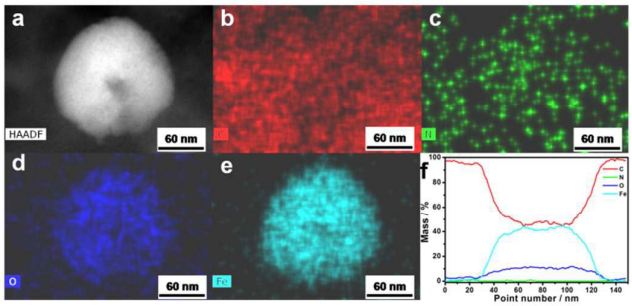


**Fig. 5** (a-e) The HAADF-STEM image, HAADF-STEM-EDS maps and (f) the cross-sectional compositional line-scanning profile of the single $Fe_3O_4$ nanocrystal.

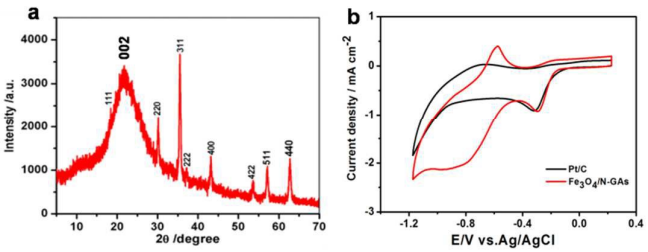


**Fig. 6** (a) The XRD pattern of $Fe_3O_4$/N-GAs; (b) Cvs of $Fe_3O_4$/N-GAs and Pt/C for ORR in $O_2$-saturated 0.1 M NaOH.

effectively loaded on the surface of graphene. Besides, the high-resolution N 1s scan result reveals that the peaks of the N-doped graphene can be fitted to three main peaks of graphitic N (401.1 eV), Fe-N (399.2 eV) and pyridinic N (398.2 eV), coinciding with literature reports that graphitic N and pyridinic N could be formed through replacement of a C atom by a N atom in the graphene plane. At the same time, N could donate electrons to Fe at the high doping temperature. More importantly, those three N states are chemically active sites for ORR (Fig. 4h).[13, 17, 52-55] The XPS of GO confirm the existence of two main types of carbon bonds: C=C (284.6 eV) and C-O (286.6 eV), respectively (Fig. S4).[13, 31] After reduction reaction, the most of oxygen-containing groups were removed and the peak associated with C=C (284.6 eV) became predominant, while the peaks related to the oxidized carbon species were greatly weakened, confirming the reduction of GO into graphene (Fig. S5). In addition, TEM EDS measurements also reveal that N atom has been doped in the aerogels (1.2 wt %, Fig. S6).

### Catalytic Performance of $Fe_3O_4$/N-GAs

The electrocatalytic properties of $Fe_3O_4$/N-GAs for ORR were first studied by cyclic voltammetry (CV). Fig. 7a presents CVs of $Fe_3O_4$/N-GAs modified electrode in the 0.1 M NaOH solution with $N_2$-saturated and $O_2$-saturated, respectively. In the presence of $O_2$, the onset potential is -0.18 V at the $Fe_3O_4$/N-GAs modified electrode, which is similar to that of commercial Pt/C (Fig. 6b).[26, 56] It is evidently that this material exhibits a significantly larger reduction current peak than Pt/C, implying an outstanding ORR catalytic performance. To discern the

contribution of individual components and the possible synergistic effects among them, control experiments on N-GAs/GC, $Fe_3O_4$ NPs/GC electrodes were also carried out. As shown in Fig. S7, the electrochemical reduction of $O_2$ on the $Fe_3O_4$ NPs/GC electrode occurs at -0.21 V. In previous reports, $Fe_3O_4$ NPs possess intrinsic peroxidase property, which would play as mimic enzymes catalysis to improve the response towards $O_2$ reduction.[57-59] In addition, the increased surface area also plays an important role in the observed increased current. At the same time, the N-GAs modified electrode exhibits much better electrocatalytic activity. The electrochemical reduction of $O_2$ already starts at -0.2 V at N-GAs/GC electrode. At approximately -0.40 V, a maximum reduction current of -0.60 mA $cm^{-1}$ is observed, and at more negative potentials, the cathodic current shows a plateau. When $Fe_3O_4$ NPs was incorporated in the N-GAs, a cathodic current density which is much larger than that of the N-GAs /GC electrode is observed, and the onset potential is slight positive shift (about 20 mV). These results demonstrated that the $Fe_3O_4$/N-GAs/GC electrode exhibited the best response towards electrochemical reduction of $O_2$. We propose that the increased cathodic current on the $Fe_3O_4$/N-GAs composite film electrode should be due to the synergistic effects between the N-GAs nanosheets and $Fe_3O_4$ NPs. Such observed synergy could be ascribed to the full contact between $Fe_3O_4$ and N-graphenes matrix, which improved electronic and ionic transport capacity and electron self-exchange in the film.[11]

To quantify the stoichiometry of the catalytic oxygen reduction, voltammetric measurements at a rotating disk electrode (RDE) and a rotating ring-disk electrode (RRDE) were performed. Fig. 7b exhibits the current-potential curves of oxygen reduction in $O_2$-saturated 0.1 M KOH solution at various rotation rates, respectively. It can be seen that one-step reduction pathway and potential-independent plateau currents are present at all rotation rates, also suggesting the synergistic effects between $Fe_3O_4$ NPs and N-GAs. Fig. 7c provides the Koutecky-Levich plot obtained from the plateau currents at -0.65 V, indicating that the ORR is a direct four-electron transfer process. A rotating GC disk-platinum ring electrode was further employed to determine the quantity of $H_2O_2$ that was generated by a two-electron reduction process of $O_2$ at the disk electrode. Fig. 7d suggests that the ratio of the ring currents to disk currents ($i_R/i_D$) is 0.0081 for the $Fe_3O_4$/N-GAs complexes.[60] According to $i_R/i_D$, the reaction electron number involved in the ORR is 3.95 (n=4-2 $i_R/(i_D N)$), where *N* is the current collection efficiency (0.37) of disk-platinum ring, being identical to that acquired from the Koutecky-Levich plot.[61] The $H_2O$ yield can be estimated as following equation (1):

$$P_{(H_2O)} = \frac{N(i_D/i_R) - 1}{N(i_D/i_R) + 1} \qquad (1)$$

From our data, the calculated $H_2O$ yield on the $Fe_3O_4$/N-GAs catalysis during oxygen reduction is 95.7%, further confirming that this ORR follows the four-electron transfer pathway with a low $H_2O_2$ yield.

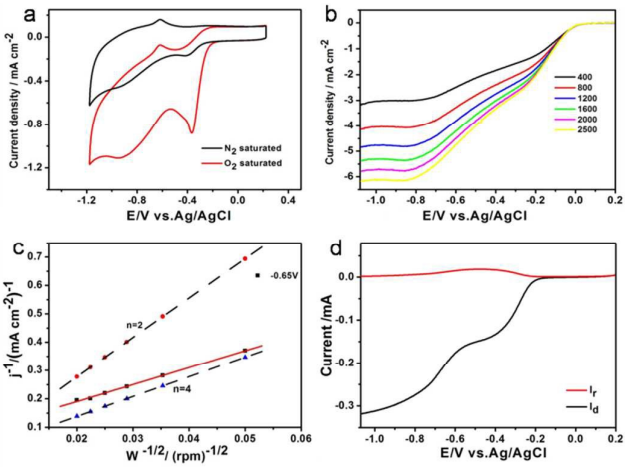


**Fig. 7** (a) CVs of $Fe_3O_4$/N-GAs as the catalyst for ORR in $N_2$ and $O_2$-saturated 0.1 M NaOH at a scan rate of 100 mV $s^{-1}$; (b) LSVs of $Fe_3O_4$/N-GAs in $O_2$-saturated 0.1 M KOH at a scan rate of 100 mV $s^{-1}$ at different RDE rotation rates (in rpm); (c) The Koutecky-Levich plot of $Fe_3O_4$/N-GAs derived from RDE tests at -0.65V; (d) The RRDE test of the $Fe_3O_4$/N-GAs in $O_2$-saturated 0.1 M KOH at a rotation rate of 100 rpm.

## Conclusions

In summary, a facile but effective protocol was developed to fabricate well-organized hybrid aerogels of $Fe_3O_4$/N-doped graphene, which obtained directly from Fc-F/GO supramolecular hydrogels through *in situ* hydrothermal treatments. Importantly, since Fc-F hydrogelator is the single precursor for both Fe and N, the association force between two new born catalytical sites ($Fe_3O_4$ NPs and N-doped sites) should be much stronger than two different precursors, which results in an ideal electron transfer tunnel for the electrochemical catalytic process. Meanwhile, GO nanosheets with abundant functional groups are able to stabilize supramolecular hydrogels and subsequently facilitate the well-distribution of $Fe_3O_4$ NPs on ultrathin graphene films. Moreover, the *in situ* formed $Fe_3O_4$ NPs can inhibit the self-aggregation among graphene sheets during the reduction of GO, which would retain many channels to allow counterions in aqueous buffers to fastly move into or out of the films and greatly enhance the charge mobility within the films. Consequently, the as-prepared hybrid aerogels exhibit high efficiency in catalyzing the electrochemical ORR (comparing to commercial Pt/C). We expect that this report can offer a new route to produce the morphology-controlled inorganic NPs in hybrid graphene nanomaterials.

## Experimental Details

### Instrumentation

SEM images were obtained by a scanning electron microscope (FEI HELIOS NanoLab 600i, America). TEM images, HAADF-STEM images and HAADF-STEM-EDS maps were

obtained from the TEM/STEM (FEI Titan G2 60-300, America), which includes corrector technologies enabling resolution of 80 pm. CD spectra measurements were used by a Jasco-815 CD spectrometer (Japan). A rotated rheometer used the AR 2000 ex TA Instrument (America). XRD measurements were performed on a D/max 2550 X-ray Power Diffractometer. XPS measurements were carried out at an ESCALAB 250Xi X-Ray Photoelectron Spectrometer (ThermoFisher-VG Scientific, America). Voltammetry measurements were performed on the CHI 650D and CHI 832C electrochemical workstations (Shanghai, China). RDE tests were used by a Pine Modulated Speed Rotator (MSR, America) with rotation rates from 50-10000 rpm.

**Synthesis of $Fe_3O_4$/N-GAs**

(a) Synthesis of Fc-F: Synthesize Fc-F as the reference did.[42]
(b) Synthesis of GO: Synthesize GO as the reference did.[62, 63] Modified Hummers methods could yield well-distributed GO solution. However, to obtain ultrathin graphene is tricky and laborious, and we usually perform a 48 hours dialysis toward GO after reducing it. But, nonetheless, we still have the loss of 30% in the process of making N-GAs.
(c) The preparation of Fc-F/GO hybrid hydrogels: The lyophilized Fc-F was dissolved in DMSO (100 mg $mL^{-1}$, as a stock solution). After the pH value of graphene oxide solution was adjusted to 7-8 by adding a small amount of PBS (10 mM, pH 9.0), the stock solution was diluted by the GO solution (a final concentration of 2 mg $mL^{-1}$ or higher). The suspension turned to be a clear brown hydrogel after incubation for several minutes.
(d) Synthesis of $Fe_3O_4$/N-GAs: The $Fe_3O_4$/N-doped GO hydrogels were prepared by incubating Fc-F/GO hybrid hydrogels through hydrothermal treatment at 180 °C for 12 h. The as-prepared $Fe_3O_4$/N-doped GO hydrogels were directly dehydrated via a freeze-drying process to form 3D aerogels and then heated at 600 °C for 3 h under nitrogen protection to obtain high performance $Fe_3O_4$/N-GAs.
(e) Synthesis of $Fe_3O_4$ and N-GAs: Synthesize $Fe_3O_4$ and N-GAs as the reference did.[64, 65]

## Acknowledgements

This work was supported by the National Natural Science Foundation of China (21473257, 91127024). This work was also supported by the Tianshan scholarship from Xinjiang University and the Key Laboratory of Food Colloids and Biotechnology, Ministry of Education, Jiangnan University, China (NO. JDSJ2013-02).

## Notes and references

1 Z. Niu, J. Chen, H. H. Hng, J. Ma and X. Chen, *Adv. Mater.*, 2012, **24**, 4144.
2 S. Yin, Y. Zhang, J. Kong, C. Zou, C. M. Li, X. Lu, J. Ma, F. Y. C. Boey and X. Chen, *ACS nano*, 2011, **5**, 3831.
3 S. Mao, G. Lu and J. Chen, *Nanoscale*, 2015, **7**, 6924.
4 Y. Y. Jiang, Y. Z. Lu, X. D. Wang, Y. Bao, W. Chen and L. Niu, *Nanoscale*, 2014, **6**, 15066.
5 J. Jiang, Y. Li, J. Liu, X. Huang, C. Yuan and X. W. Lou, *Adv. Mater.*, 2012, **24**, 5166.
6 M. Lefevre, E. Proietti, F. Jaouen and J. P. Dodelet, *Science*, 2009, **324**, 71.
7 S. Guo, D. Li, H. Zhu, S. Zhang, N. M. Markovic, V. R. Stamenkovic and S. Sun, *Angew. Chem. Int. Ed.*, 2013, **52**, 3465.
8 W. Liu, P. Rodriguez, L. Borchardt, A. Foelske, J. P. Yuan, A. K. Herrmann, D. Geiger, Z. K. Zheng, S. Kaskel, N. Gaponik, R. Kotz, T. J. Schmidt and A. Eychmuller, *Angew. Chem. Int. Ed.*, 2013, **52**, 9849.
9 S. Guo and S. Sun, *J. Am. Chem. Soc.*, 2012, **134**, 2492.
10 D. Wen, A. K. Herrmann, L. Borchardt, F. Simon, W. Liu, S. Kaskel and A. Eychmuller, *J. Am. Chem. Soc.*, 2014, **136**, 2727.
11 G. Wu, N. H. Mack, W. Gao, S. Ma, R. Zhong, J. Han, J. K. Baldwin and P. Zelenay, *ACS Nano*, 2012, **6**, 9764.
12 C. K. Chua, A. Ambrosi, Z. Sofer, A. Macková, V. Havránek, I. Tomandl and M. Pumera, *Chem. Eur. J.*, 2014, **20**, 15760.
13 S. A. Wohlgemuth, R. J. White, M. G. Willinger, M. M. Titirici and M. Antonietti, *Green Chem.*, 2012, **14**, 1515.
14 Z. Juanjuan, L. Ruiyi, L. Zaijun, L. Junkang, G. Zhiguo and W. Guangli, *Nanoscale*, 2014, **6**, 5458.
15 C. Wang, Y. Li, X. He, Y. Ding, Q. Peng, W. Zhao, E. Shi, S. Wu and A. Cao, *Nanoscale*, 2015, **7**, 7550.
16 W. Wei, S. B. Yang, H. X. Zhou, I. Lieberwirth, X. L. Feng and K. Mullen, *Adv. Mater.*, 2013, **25**, 2909.
17 S. Yang, X. Feng, X. Wang and K. Müllen, *Angew. Chem. Int. Ed.*, 2011, **50**, 5339.
18 J. Luo, J. Liu, Z. Zeng, C. F. Ng, L. Ma, H. Zhang, J. Lin, Z. Shen and H. J. Fan, *Nano Lett.*, 2013, **13**, 6136.
19 Y. Zhao, C. G. Hu, Y. Hu, H. H. Cheng, G. Q. Shi and L. T. Qu, *Angew. Chem. Int. Ed.*, 2012, **51**, 11371.
20 Y. Zhu, B. Zhang, X. Liu, D. Wang and D. S. Su, *Angew. Chem. Int. Ed.*, 2014, **53**, 10673.
21 G. Zhou, D. Wang, F. Li, L. Zhang, N. Li, Z. Wu, L. Wen, G. Lu and H. Cheng, *Chem. Mater.*, 2010, **22**, 5306.
22 J. Xu, P. Gao and T. S. Zhao, *Energy Environ. Sci.*, 2012, **5**, 5333.
23 Y. Meng, W. Song, H. Huang, Z. Ren, S. Chen and S. L. Suib, *J. Am. Chem. Soc.*, 2014, **136**, 11452.
24 H. T. Chung, J. H. Won and P. Zelenay, *Nat. Commun.*, 2013, **4**, 1922.
25 X. W. Lou, D. Deng, J. Y. Lee, J. Feng and L. A. Archer, *Adv. Mater.*, 2008, **20**, 258.
26 Z. Wu, S. Yang, Y. Sun, K. Parvez, X. Feng and K. Müllen, *J. Am. Chem. Soc.*, 2012, **134**, 9082.
27 M. Sun, H. Liu, Y. Liu, J. Qu and J. Li, *Nanoscale*, 2015, **7**, 1250.
28 Y. Liang, Y. Li, H. Wang, J. Zhou, J. Wang, T. Regier and H. Dai, *Nat. Mater.*, 2011, **10**, 780.
29 L. Li, H. B. Wu, L. Yu, S. Madhavi and X. W. Lou, *Adv. Mater. Interfaces*, 2014, DOI: 10.1002/admi.201400050.
30 H. Li, L. Liu and F. Yang, *J. Mater. Chem.*, 2013, **1**, 3446.

31 W. Chen, S. Li, C. Chen and L. Yan, *Adv. Mater.*, 2011, **23**, 5679.
32 Z. Wu, Y. Sun, Y. Tan, S. Yang, X. Feng and K. Müllen, *J. Am. Chem. Soc.*, 2012, **134**, 19532.
33 S. Chen and S. Qiao, *ACS Nano*, 2013, **7**, 10190.
34 X. Wang, W. Tian, D. Liu, C. Zhi, Y. Bando and D. Golberg, *Nano Energy*, 2013, **2**, 257.
35 Y. Liang, H. Wang, J. Zhou, Y. Li, J. Wang, T. Regier and H. Dai, *J. Am. Chem. Soc.*, 2012, **134**, 3517.
36 X. Y. Zhang, X. Chen, K. J. Zhang, S. P. Pang, X. H. Zhou, H. X. Xu, S. M. Dong, P. X. Han, Z. Y. Zhang, C. J. Zhang and G. L. Cui, *J. Mater. Chem. A*, 2013, **1**, 3340.
37 J. Duan, S. Chen, S. Dai and S. Z. Qiao, *Adv. Funct. Mater.*, 2014, **24**, 2072.
38 S. Bag, K. Roy, C. S. Gopinath and C. R. Raj, *ACS Appl. Mater. Interfaces*, 2014, **6**, 2692.
39 L. Barišić, M. Čakić, K. A. Mahmoud, Y. Liu, H. B. Kraatz, H. Pritzkow, S. I. Kirin, N. Metzler Nolte and V. Rapić, *Chem. Eur. J.*, 2006, **12**, 4965.
40 S. I. Kirin, H. B. Kraatz and N. Metzler Nolte, *Chem. Soc. Rev.*, 2006, **35**, 348.
41 X. Yan, P. Zhu and J. Li, *Chem. Soc. Rev.*, 2010, **39**, 1877.
42 Z. F. Sun, Z. Y. Li, Y. H. He, R. J. Shen, L. Deng, M. H. Yang, Y. Z. Liang and Y. Zhang, *J. Am. Chem. Soc.*, 2013, **135**, 13379.
43 S. Debnath, S. Roy and R. V. Ulijn, *J. Am. Chem. Soc.*, 2013, **135**, 16789.
44 S. Fleming, S. Debnath, P. W. J. M. Frederix, N. T. Hunt and R. V. Ulijn, *Biomacromolecules*, 2014, **15**, 1171.
45 W. Miao, D. Yang and M. Liu, *Chem. Eur. J.*, 2015, **21**, 7562.
46 H. Cong, X. Ren, P. Wang and S. Yu, *ACS Nano*, 2012, **6**, 2693.
47 Z. Fan, W. Kai, J. Yan, T. Wei, L. Zhi, J. Feng, Y. Ren, L. Song and F. Wei, *ACS Nano*, 2010, **5**, 191.
48 X. H. Cao, B. Zheng, X. H. Rui, W. H. Shi, Q. Y. Yan and H. Zhang, *Angew. Chem. Int. Ed.*, 2014, **53**, 1404.
49 H. Cong, J. Chen and S. Yu, *Chem. Soc. Rev.*, 2014, **43**, 7295.
50 Y. Y. Ma, Q. Kuang, Z. Y. Jiang, Z. X. Xie, R. B. Huang and L. S. Zheng, *Angew. Chem. Int. Ed.*, 2008, **47**, 8901.
51 W. Ding, Z. Wei, S. Chen, X. Qi, T. Yang, J. Hu, D. Wang, L. Wan, S. F. Alvi and L. Li, *Angew. Chem.*, 2013, **125**, 11971.
52 Z. Wu, A. Winter, L. Chen, Y. Sun, A. Turchanin, X. Feng and K. Müllen, *Adv. Mater.*, 2012, **24**, 5130.
53 L. Lin, Q. Zhu and A. Xu, *J. Am. Chem. Soc.*, 2014, **136**, 11027.
54 G. Wu, C. M. Johnston, N. H. Mack, K. Artyushkova, M. Ferrandon, M. Nelson, J. S. Lezama Pacheco, S. D. Conradson, K. L. More, D. J. Myers and P. Zelenay, *J. Mater. Chem.* , 2011, **21**, 11392.
55 H. Yin, C. Zhang, F. Liu and Y. Hou, *Adv. Funct. Mater.*, 2014, **24**, 2930.
56 A. Shen, Y. Zou, Q. Wang, R. A. W. Dryfe, X. Huang, S. Dou, L. Dai and S. Wang, *Angew. Chem. Int. Ed.*, 2014, **53**, 10804.
57 J. Gao, H. Gu and B. Xu, *Acc. Chem. Res.*, 2009, **42**, 1097.
58 H. Wei and E. Wang, *Anal. Chem.*, 2008, **80**, 2250.
59 L. Gao, J. Zhuang, L. Nie, J. Zhang, Y. Zhang, N. Gu, T. Wang, J. Feng, D. Yang, S. Perrett and X. Yan, *Nat. Nanotechnol.*, 2007, **2**, 577.
60 M. Huang, Y. Shao, X. Sun, H. Chen, B. Liu and S. Dong, *Langmuir*, 2004, **21**, 323.
61 S. Liu, J. Xu, H. Sun and D. Li, *Inorg. Chim. Acta*, 2000, **306**, 87.
62 Y. Liu, Y. Zhang, G. Ma, Z. Wang, K. Liu and H. Liu, *Electrochim. Acta*, 2013, **88**, 519.
63 W. S. Hummers and R. E. Offeman, *J. Am. Chem. Soc.*, 1958, **80**, 1339.
64 H. Hu, Z. Zhao, W. Wan, Y. Gogotsi and J. Qiu, *Adv. Mater.*, 2013, **25**, 2219.
65 L. Y. Wang, J. Bao, L. Wang, F. Zhang and Y. D. Li, *Chem. Eur. J.*, 2006, **12**, 6341.